

Type-IV Antifreeze Proteins are Essential for Epiboly and Convergence in Gastrulation of Zebrafish Embryos

Qing Xiao*, Jian-Hong Xia*, Xiao-Juan Zhang, Zhi Li, Yang Wang, Li Zhou, Jian-Fang Gui[✉]

State Key Laboratory of Freshwater Ecology and Biotechnology, Institute of Hydrobiology, Chinese Academy of Sciences, University of the Chinese Academy of Sciences, Wuhan 430072, China.

*These authors contributed equally to this work.

[✉] Corresponding author: Tel: +86-27-68780707; Fax: +86-27-68780123; E-mail: jfgui@ihb.ac.cn.

© Ivyspring International Publisher. This is an open-access article distributed under the terms of the Creative Commons License (<http://creativecommons.org/licenses/by-nc-nd/3.0/>). Reproduction is permitted for personal, noncommercial use, provided that the article is in whole, unmodified, and properly cited.

Received: 2014.03.16; Accepted: 2014.05.18; Published: 2014.06.24

Abstract

Many organisms in extremely cold environments such as the Antarctic Pole have evolved anti-freeze molecules to prevent ice formation. There are four types of antifreeze proteins (AFPs). Type-IV antifreeze proteins (AFP4s) are present also in certain temperate and even tropical fish, which has raised a question as to whether these AFP4s have important functions in addition to antifreeze activity. Here we report the identification and functional analyses of AFP4s in cyprinid fish. Two genes, namely *afp4a* and *afp4b* coding for AFP4s, were identified in gibel carp (*Carassius auratus gibelio*) and zebrafish (*Danio rerio*). In both species, *afp4a* and *afp4b* display a head-to-tail tandem arrangement and share a common 4-exonic gene structure. In zebrafish, both *afp4a* and *afp4b* were found to express specifically in the yolk syncytial layer (YSL). Interestingly, *afp4a* expression continues in YSL and digestive system from early embryos to adults, whereas *afp4b* expression is restricted to embryogenesis. Importantly, we have shown by using *afp4a*-specific and *afp4b*-specific morpholino knockdown and cell lineage tracing approaches that AFP4a participates in epiboly progression by stabilizing yolk cytoplasmic layer microtubules, and AFP4b is primarily related to convergence movement. Therefore, both AFP4 proteins are essential for gastrulation of zebrafish embryos. Our current results provide first evidence that AFP such as AFP4 has important roles in regulating developmental processes besides its well-known function as antifreeze factors.

Key words: antifreeze protein; yolk syncytial layer; epiboly; convergence; morphogenesis.

Introduction

During vertebrate embryogenesis, embryonic cell movements are very critical for morphogenesis and establishment of normal embryo architecture [1]. Through this process, the blastoderm transforms into three germ layers of endoderm, mesoderm and ectoderm as well as two major body axes of anterior-posterior axis and ventral-dorsal axis, and these changes mainly result from the harmonized morphogenetic movements, including epiboly, involution, convergence and extension (CE) [2, 3]. Numerous studies have shed light on some signaling molecules [3, 4], and some key factors that are related to cell adhesion, cytoskeletal rearrangement and cell inter-

actions between the enveloping layer (EVL) and the yolk syncytial layer (YSL) have been suggested to play significant roles in gastrulation cell movements and embryonic development [5]. For example, the lipid pregnenolone, produced from cholesterol by Cyp11a1 enzyme, was shown to promote zebrafish (*Danio rerio*, *Dr*) embryonic cell movements by increasing yolk cytoplasmic layer (YCL) microtubule abundance [6]. In addition, Npc1 (Niemann-Pick disease, type C1), a 13 transmembrane-spanning protein containing a sterol-sensing domain, was also demonstrated to contribute early morphogenetic movements including epiboly and CE movements [7]. Neverthe-

less, most of the significant regulators remain to be further identified because embryonic cell movements have been believed to be driven by a variety of cellular behaviors and other molecules [8].

Following our systematic studies on maternal factor screening and gene function identification [9-13] in polyploid gibel carp (*Carassius auratus gibelio*, *Cag*) with multiple modes of unisexual and sexual reproduction [14-19], we have also identified and characterized a type-IV antifreeze protein gene (*afp4*) [20]. Antifreeze proteins (AFPs) have been found in fungi, bacteria, plants and animals, and they can bind to ice crystals to inhibit growth and recrystallization of ice [21]. According to their molecular structures, four types of AFPs, type I-IV AFPs, have been characterized in teleost fishes [22]. The type-IV antifreeze protein (AFP4) was firstly discovered from longhorn sculpin (*Myoxocephalus octodecemspinosis*) in 1997 [23], and its homologues had been identified in other teleost fishes, ranging from polar to tropic region and from seawater to freshwater [20, 24, 25]. As a new type of AFP, their molecular structures have been characterized by the conserved four-helix bundle [24-26], and the antifreeze activity has been demonstrated in several fishes [23-26]. Significantly, along with wide discoveries of *afp4* homologues, their abundant expression has been detected recently in oocytes [27, 28] and in embryos [20] from some teleost fishes. So far, AFPs have been studied for more than 30 years, but almost all the previous studies have focused on the structural and biochemical properties in freezing avoidance [29-31], and little is known about the biological functions in embryonic development. The finding about abundant expression of *afp4* during embryogenesis in gibel carp provides a good chance for us to explore the biological roles. In this study, we firstly identify two tandem duplicated *afp4* genes from gibel carp and zebrafish, analyze their genomic organization, and characterize their expression pattern. Then, we use zebrafish as a model to reveal their biological functions as two key regulators in early morphogenetic movements of zebrafish embryogenesis.

Materials and Methods

Full-length cDNA cloning

A positive BAC clone of *afp4* was isolated from gibel carp BAC library [32] by PCR screening based on the cDNA sequence of *afp4* in gibel carp (*Cagafp4*, GenBank accession No. AY365004) and it was sequenced as described previously [10]. Zebrafish database search was performed on the web server of NCBI by BLAST using the cDNA of *Cagafp4* as a query

of nucleotide collection (nr/nt) database.

To achieve full-length cDNA sequence of the other *Cagafp4* (*Cagafp4a*) and reexamine those of *afp4s* in zebrafish (*Drafp4s*), total RNAs of gibel carp or zebrafish embryos were purified with TRIzol Reagent (Ambion, USA) as described previously [33], and then SMART cDNA libraries were constructed according to the SMARTer™ PCR cDNA Synthesis Kit User Manual (Clontech, USA). The *Cagafp4a* and *Drafp4s* cDNAs were completed by 3' and 5' rapid amplification of cDNA ends (RACE), with primers (Table 1) based on the obtained *Cagafp4s* or *Drafp4s* cDNA sequences. The complete cDNA sequences of *Cagafp4a* and *Drafp4a* were deposited in GenBank (accession No. KJ183062 and KJ183061, respectively).

Sequence and phylogenetic analyses

The genomic structures of *Cagafp4s* and *Drafp4s* were achieved by comparative analyses between cDNA sequences and corresponding genomic sequences.

The complete sequences of other functionally characterized AFP4s in *Myoxocephalus octodecemspinosis* (Mo) [23, 26], *Pleuragramma antarcticum* (Pa), *Notothenia coriiceps* (Nc) [25] and *Gadus morhua* (Gm) [27, 28] were downloaded from GenBank non-redundant protein database. An unrooted maximum likelihood (ML) phylogenetic tree of AFP4s was constructed by MEGA 6 [34] with 1000 bootstrap replications, in which their evolutionary distances were computed using the JTT+F model, which was selected by ProtTest 2.4 [35] based on the corrected Akaike information criterion. Multiple amino acid sequence alignment was performed by Clustalx program (EMBL-EBI, UK). Signal peptides were predicted by a web tool SignalP 3.0 Server (CBS, Denmark). Identities and similarities between *DrAFP4a* and the other seven AFP4s were acquired by pairwise alignment using a web tool EMBOSS Needle (EMBL-EBI, UK). Sequence alignment of *Drafp4a* and *Drafp4b* cDNA was performed by DNAMAN 6.0 software (Lynnon Biosoft, Canada).

Zebrafish manipulation

Wild type (WT) zebrafish were maintained as described by Westerfield, and all the zebrafish embryos were obtained from natural spawning, and rinsed with embryos medium [36]. Embryos were incubated at 28.5°C and staged according to Kimmel et al [2]. The animal protocol for this research was approved by the Institute of Hydrobiology Institutional Animal Care and Use Committee (Approval ID: keshuizhuan 0829).

Table 1. Primers used in this study.

Name	Sequence (5'→3')	Usage
<i>Cagafp4a</i> -5'Race	AACCAGCATACATACGAAGAG	RACE
<i>Cagafp4a</i> -3'Race	TTCCTCATCGCTGTCCTTGTAC	
<i>Draf4a</i> -5'Race	CAGAGGCTTGATCTGCTCT	
<i>Draf4a</i> -3'Race	CAATCTGGACCAAGG	
<i>Draf4b</i> -5'Race	GGCAATAGGTTAACATCTGGTCC	
<i>Draf4b</i> -3'Race	TATCGTCACATTGACACAAGG	
5' PCR Primer	AAGCAGTGGTATCACCGCAGAGTAC	
3' PCR Primer	AAGCAGTGGTATCACCGCAGAGTACTTTT	
<i>Drβ</i> -actin-F	AGCACGGTATTGTGACTAATG	qPCR and semi-quantitative RT-PCR
<i>Drβ</i> -actin-R	TCGAACATGATCTGTCATC	
<i>Draf4a</i> -RT-F	CAATCTGGACCAAGG	
<i>Draf4a</i> -RT-R	CAGAGGCTTGATCTGCTCT	
<i>Draf4b</i> -RT-F	TATCGTCACATTGACACAAGG	
<i>Draf4b</i> -RT-R	GGCAATAGGTTAACATCTGGTCC	
<i>Draf4a</i> -WISH-F	TCTGGACGCAAGGCAACT	WISH
<i>Draf4a</i> -WISH-R	TCTAATACGACTCACTATAGGGAAACAAAACCATCAGCATAAC	
<i>Draf4b</i> -WISH-F	AGAGCCCAGTTTCAGCCCAT	
<i>Draf4b</i> -WISH-R	TAATACGACTCACTATAGGGACAATCAACTCCAAAATATCAGG	
<i>Draf4a</i> -EGFP-F	GGATCCTCTGGACGCAAGGCAACT	Synthesizing <i>afp4</i> :EGFP mRNA
<i>Draf4a</i> -EGFP-R	AAGCTTGGCCTGGTCAGCAACAAAT	
<i>Draf4b</i> -EGFP-F	GGATCCGACACACCACACGACA	
<i>Draf4b</i> -EGFP-R	AAGCTTCTCTGCTCTCCAGGTAAG	
EGFP-F	AAGCTTATGGTGAGCAAGGGCGA	
EGFP-R	CTCGAG TTACTTGTACAGCTCGTCCAT	
<i>Draf4a</i> -F	TGGATCCATGAAATTCTCCCTCATCG	Synthesizing <i>afp4</i> mRNA
<i>Draf4a</i> -R	CGCTCGAGAAACAAAACCATCAGCATAAC	
<i>Draf4b</i> -F	TGGATCCATGAAACTCTCCCTCATC	
<i>Draf4b</i> -R	CGCTCGAGGGATACTCATATCTGGAG	

RNA isolation, real-time PCR and semi-quantitative RT-PCR

Total RNAs were isolated from zebrafish embryos or tissues of adults using TRIzol Reagent as described previously [33], and cDNAs were then generated using M-MLV Reverse Transcriptase (Promega, USA) as described previously [37]. Real-time PCR (qPCR) and semi-quantitative RT-PCR analyses were performed with specific primers for *afp4a*, *afp4b* and *β*-actin (Table 1) as described previously [37, 38].

Western blot analyses

Western blot analyses were performed as reported previously using the anti-CagAfp4 antibody (1:200) [20]. Immunoreactive bands were visualized by using BCIP/NBT staining.

Whole-mount *in situ* hybridization

Whole-mount *in situ* hybridization (WISH) was carried out as previously described [39]. For antisense probe synthesis, T7 RNA polymerase promoter was added to the 5' end of reverse primers and a DIG RNA labeling kit (Roche, Germany) was used. In brief,

DNA templates of *Draf4a/b* were amplified by RT-PCR from zebrafish embryos cDNA with the primers *Draf4a/b*-WISH-F and *Draf4a/b*-WISH-R (Table 1). The riboprobe produced for *Draf4a* was targeted to nucleotides 20-525 (accession No. KJ183061) and for *Draf4b* to nucleotides 292-844 (accession No. BC153962). In addition, antisense probes of the following mRNAs were synthesized and used: *foxA3*, *gsc*, *ntl*, *myoD*, *hgg1*, *dxl3b*, *pax2.1*, *sox17*, *eve1*. For sectioning, 15 µm sections of the stained shield to bud stage embryos were made on a CM 1850 frozen microtomy (Leica, Germany) according to the previous report [40]. Images were acquired by Leica S8APO dissecting microscope (Leica, Germany). To measure the extent of epiboly or mediolateral length of somites, the pictures of embryos stained by *ntl* probe or *myoD* probe were measured by ImageJ software 1.47v (National Institutes of Health, USA) and analyzed as described previously [6, 41].

Morpholinos, RNAs and microinjection

Morpholinos (MOs, Gene Tools, LLC, USA) were designed to target the 5' untranslated region (tb-MO) or the intron 3/ exon 4 boundary (sb-MO) of *Draf4a* or *Draf4b*. Sequences were as following: *afp4a*-tb-MO:

5'-AAGAGTTGCCCTGCGTCCAGAGATT-3'; *afp4a*-sb-MO: 5'-CACTGTGCCATGAACAAACAAAAAC-3'; *afp4b*-tb-MO: 5'-ATGATTGTGGATGAGCCAGG GTTG-3'; *afp4b*-sb-MO: 5'-AAGCACTGCATCACAA AGACAATAC-3'. In addition, several control MOs, such as standard control MO (Ctrl-MO, 5'-CCTCCTACCTCAGTTACAATTATA-3'), *afp4a*-sb-miMO (*afp4a*-sb-MO with five-nucleotide mismatches indicated in lowercase, 5'-CACTcTcCCATG AAgAAAtCtAAAAC-3'), and *afp4b*-tb-miMO (*afp4b*-tb-MO with five-nucleotide mismatches indicated in lowercase, 5'-ATcATTGTcGGATcAGCCAcGcTTG-3') were also synthesized.

For rescue experiments, *afp4a* and *afp4b* cDNAs were amplified with primers containing BamHI and XhoI restriction sites from full-length cDNA without 5' untranslated region (UTR) and cloned into pCS2+. To test the efficiency and specificity of tb-MOs, 5' UTR and part of the N-terminal open reading frame (ORF) of *afp4a* or *afp4b* were fused in frame with the EGFP ORF, and cloned into pCS2+ (primers are listed in Table 1). Plasmid for *in vitro* transcription of Kaede was generous gift from Dr. Brian Ciruna. Capped RNAs were prepared with the mMESSAGE mMACHINE kit (Ambion, USA) as previously described [12].

MOs or mRNAs were injected at the one-cell stage. The amount of MO or mRNA injected for each embryo was as below: *afp4a*-sb-MO or *afp4a*-sb-miMO, 4 ng; *afp4b*-tb-MO or *afp4b*-tb-miMO, 2.5 ng; *afp4a*-tb-MO or *afp4b*-sb-MO, 8 ng; *afp4*-MOs, 4 ng *afp4a*-sb-MO and 2.5 ng *afp4b*-tb-MO; Ctrl-MO was at the same amount with *afp4*-MO using in the same experiment; to detect the translation blocking efficiency, about 100 pg *afp4a*:EGFP or *afp4b*:EGFP mRNA was injected into a random subset of *afp4*-MO-injected embryos (co-injection); for rescue experiment, about 150 pg *afp4a* or *afp4b* mRNA was co-injected with *afp4*-MO.

Reagent treatments

For nocodazole treatment, the dechorionated embryos were incubated in 1 µg/mL nocodazole (Sigma, USA), which was diluted in 1 x Danieau buffer as previously described [6]. For pregnenolone treatment, the dechorionated embryos were incubated with 0.1, 1, 10 or 20 µM pregnenolone (Sigma, USA) from 1k-cell stage until the late epiboly stage.

Microtubule and F-actin staining

Embryos with chorion removed were fixed in microtubule-stabilizing buffer (MSB) and the whole-mount microtubule staining with primary antibody mouse anti-β-tubulin (1:500 in blocking buffer, Sigma, USA) and secondary antibody rhoda-

mine-conjugated goat anti-mouse IgG (1:200 in blocking buffer, Thermo, USA) was performed according to previous study [42].

Images were acquired with a Leica TCS-SP2 confocal microscope (Leica, Germany), and confocal Z-series image stacks collected at 2 µm intervals were assembled by LSM510 basic software. Microtubule area percentage (%) was calculated as following steps. Firstly, several 100 x 100 pixel (about 72.2 x 72.2 µm) images of the YCL microtubules were randomly intercepted from the blastoderm margin of each embryo picture, as indicated by a white square in the corresponding picture. Then, these images were changed to gray-scale images by Adobe Photoshop CS (Adobe, USA). Moreover, the gray-scale images were converted to white (microtubules) and black (background) by Make Binary of ImageJ. Finally, the pixel number of white (n) in each image was measured by Histogram of ImageJ, and the proportion in the 100 x 100 pixel (n/10000) was computed as microtubule area percentage (%) in each image. For this calculation, more than 20 embryos were used, and about five images for each embryo were computed.

F-actin staining was carried out with 1 µg/mL rhodamine-phalloidin (Sigma, USA) as previously described [43]. Rhodamine-phalloidin was prepared as stock solutions of 1 mg/mL in methanol, and then diluted in PBTD/BSA just before use. Images were acquired with a Leica TCS-SP2 confocal microscope and confocal Z-series image stacks collected at 2 µm intervals were assembled by LSM510 basic software. Phalloidin signal intensity, which indicated F-actin intensity, was analyzed using ImageJ software as previously described [44].

Cell lineage tracing

Cell lineage tracing was performed according to previous reports [41, 45]. Briefly, 100 pg Kaede mRNA was injected with *afp4b*-tb-miMO or *afp4b*-tb-MO to embryos at the one-cell stage. The injected embryos were kept in the dark until the shield stage. The Kaede fluorophore was converted from green to red by focusing a 40-sec pulse of ultraviolet (UV) light, specifically on a group of cells in dorsal or lateral blastoderm margin, using the pinhole of a Leica LCS SP2 confocal microscope. Photos were acquired at the indicated developmental stages by a Leica MZ16 FA stereomicroscope (Leica, Germany). Figures were constructed using Adobe Photoshop CS. The angle and length were measured by utilizing ImageJ software.

Statistical analyses

For statistical analyses, means ± standard deviation (SD) were acquired by Microsoft Excel 2003 (Mi-

crosoft, USA), and one-way analyses of variance (ANOVA) and cross-table analyses were performed with SPSS 13.0 software (SPSS, USA).

Results

Identification and molecular characterization of two tandem *afp4s* in gibel carp and zebrafish

Previous report has characterized a full-length cDNA of *afp4* in gibel carp (GenBank accession No. AY365004) [20]. To characterize its genomic organization, we obtained a positive BAC by PCR screening from gibel carp BAC library [32] as described previously [10]. Sequencing the BAC clone revealed the two tandem duplicated gene sequences, and full-length cDNA of the other *afp4* was achieved by RACE (GenBank accession No. KJ183062). Zebrafish database searches also found a similar genomic organization of the two tandem duplicated genes on the chromosome 16 (Supplementary material Fig. S1), and revealed two *afp4* homologues (GenBank accession No. BC133822 and BC153962). Then, full-length cDNAs of the two *afp4s* was reexamined and acquired by RACE (GenBank accession No. KJ183061 and BC153962). Genomic organization comparison between gibel carp and zebrafish revealed almost identical exons in size and similar exon/intron boundaries (Supplementary material Table S1).

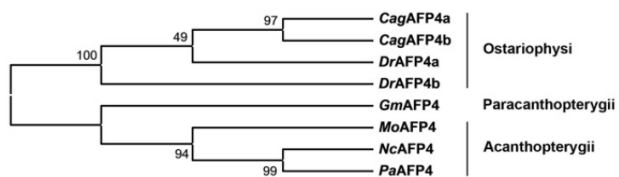
In order to clarify evolutionary relationship between the four AFPs and other functionally characterized AFP4s with antifreeze activity, we constructed a phylogenetic tree. As shown in Fig. 1A, although the classification position of these species belongs to different orders including Ostariophysi, Paracanthopterygii and Acanthopterygii, the eight known AFP4s are gathered into two main clades. Clade A contains *DrAFP4s* and *CagAFP4s*, and clade B includes the four functionally characterized AFP4s. Multiple amino acid sequence alignment of *DrAFP4s* and other AFP4s also revealed their evolutionary conservation. Significantly, the newly characterized AFPs in zebrafish and gibel carp shared common properties of the functionally characterized AFP4s, including the four α -helical regions, signal peptide, unrelated coding region 1 and 2 (UCR1 and UCR2), the 33-codon block, and 11-mer repeats [23-26]. Moreover, the amino acid identities between *DrAFP4a* and other AFP4 ranged from 31.1% to 83.8%, and their signal peptide and α -helical region showed higher consensus than the complete amino acid sequences (Fig. 1B). Therefore, the newly identified and characterized genes should belong to homologs of *afp4*. *Drafp4a* and *Drafp4b* were abbreviated to *afp4a* and *afp4b* for the common use.

To further investigate the biological functions of *afp4s* in zebrafish, we analyzed the full-length cDNA sequences of zebrafish *afp4a* and *afp4b* (GenBank accession No. KJ183061 and BC153962, respectively). As shown in Fig. 1C, their nucleotide sequence alignment shows 88.8% of high identity in the ORFs, but much lower identity exists in the 5' and 3' UTR regions, and the 3' UTR of *afp4b* is 275 nt longer than that of *afp4a*. Moreover, significant sequence differences were found in their predicted promoter regions in 5' upstream sequences (data not shown). All the sequence differences imply the existence of their divergence in expression pattern and biological function.

Divergent and dynamic temporal expression patterns between *afp4a* and *afp4b*

Subsequently, we examined expression patterns of *afp4a* and *afp4b* in zebrafish by qPCR and Western blot analyses. Firstly, two sets of specific primers were designed according to their most divergent sequences to detect and distinguish *afp4a* transcript and *afp4b* transcript, respectively (Fig. 1C), and the transcript specificity was verified by sequencing the amplified products of *afp4a* and *afp4b*. Significantly, the qPCR revealed differential expression pattern and dynamic changes between *afp4a* and *afp4b* during embryogenesis and early larval development. As shown in Fig. 2A, *afp4a* initially transcribes from 4 hours postfertilization (hpf) at which the embryos develop to sphere stage, whereas *afp4b* transcribes from 6 hpf when the embryos are at shield stage. As development proceeds, *afp4a* transcript increases progressively and reaches to the highest level at 12 hpf when the embryos develop to 6-somite stage, whereas the amount of *afp4b* transcript exceeds that of *afp4a* at 12 hpf, and peaks at 16 hpf. At the *afp4b* peak duration, *afp4a* transcript gradually decreases from 12 hpf to 20 hpf. Then, when the *afp4b* transcript reduces gradually from 20 hpf to 28 hpf, *afp4a* transcript rises again from 24 hpf to 28 hpf. Around 32 hpf, *afp4b* increases again, and quickly declines to the bottom from 32 hpf to 48 hpf. After 48 hpf, almost no *afp4b* transcript is detected in the later embryos and larvae. However, the *afp4a* transcript decreases again from 32 hpf to 72 hpf, but its transcript gains once again in 96 hpf and 120 hpf larvae. The AFP4s protein expression pattern during embryogenesis was also detected by Western blot assay using the antibody against both AFP4s. As shown in Fig. 2B, the specific AFP4s protein band appears from 6 hpf at shield stage, reaches to the peak level at 16 hpf, and then reduces gradually to a certain level from 24 hpf to 96 hpf during later embryogenesis.

A



B

	CD linker	D	Identity (%)	Similarity (%)
DrAFP4a	PLAASVQSQVA PLAGMVQTHVE DMIKFVADQAKAMLPPQ	130		
DrAFP4b	PIAASVQAQVA PLADIVQTHIE DVLKFVADKTKTILPPQ	129	83.1	92.3
CagAFP4a	PLAASVQAQVA PLASMIQTHVE DVLKFVADTSKAILPQ-	129	81.5	89.2
CagAFP4b	PLAASVQAQVA PLASMIQTHVE DVLKFVADKSKAILPPQ	130	83.8	93.1
NcAFP4	PLAANVQAQFQ PQIDSFQQQQID AIMQQQLTRPAAPIAN--	128	33.8	59.6
PaAFP4	PLAANVQAQFQ PQIDSFQQQQME AIFQQQLTRPAAPIDN--	128	35.3	58.1
MoAFP4	PLTANVQAHLQ PQIDNFQKQME AIKKLITDQTMAIEN--	128	36.8	59.6
GmAFP4	PLAEDMQKKLK PYVDEFQSELE SVLRKLDDQAKAITQ--	125	31.1	59.8
Consensus	*:: .::* :. * . * .:: .:: : .:: .: 7.....8..... 9..... .UCR2 Exon 4.....			

C

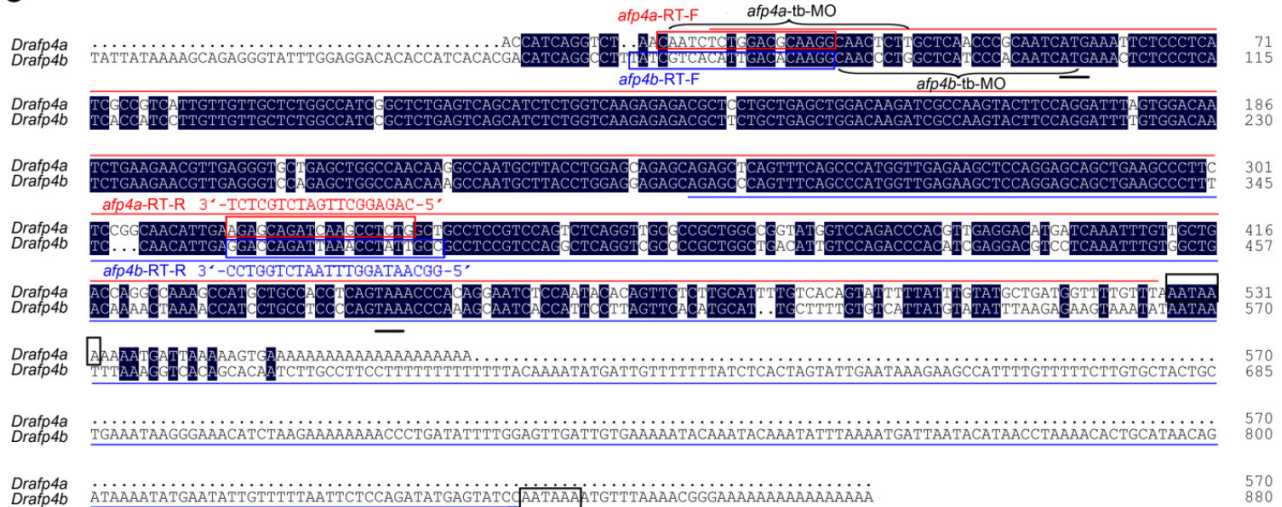


Figure 1. Phylogenetic relationship and molecular characterization of DrAFP4s and other functionally characterized AFP4s. (A) An unrooted ML phylogenetic tree of the known AFPs from *Danio rerio* (DrAFP4a, NP_001038953; DrAFP4b, XP_697091), *Carassius auratus gibelio* (CagAFP4a, AHZ08737; CagAFP4b, AAR12991), *Gadus morhua* (GmAFP4, Q56TU0), *Myoxocephalus octodecemspinosis* (MoAFP4, ABA41379), *Notothenia coriiceps* (NcAFP4, ADU02181) and *Pleuragramma antarcticum* (PaAFP4, ADU02180). Their classification positions, such as Ostariophysi, Paracanthopterygii and Acanthopterygii, are indicated on the right. (B) Multiple amino acid sequence alignment of DrAFP4s and other AFP4s. Amino acids consensus is shown below the alignment by three kinds of consensus symbols. An asterisk (*) means a position where has a single conserved residue; a colon (:) means a position where process high similarity (scoring > 0.5); a period (.) means a position where hold low similarity (scoring = < 0.5). Asterisks (*) above protein sequences show the predicate α -helical regions. Three exons (E2, E3 and E4) and boundary of eight parts of proteins [signal peptide, unrelated coding region I and 2 (UCR1 and UCR2), the 33-codon block, and I I-mer repeats (4 to 9)] are indicated according to a previous report [25]. Identities and similarities between DrAFP4a with other AFP4s are shown behind the alignment. (C) Nucleotide sequence alignment of *Draf4a* and *Draf4b* cDNAs. Identical nucleotides are indicated by the black background; the start code (ATG) and stop code (TAA) are lined by black lines; putative polyadenylation signals are boxed; the targets of the antisense probe to *afp4a* or *afp4b* used in whole-mount *in situ* hybridization are lined by red line above or blue line below sequences, respectively; two sets of specific primers used in RT-PCR to detect *afp4a* or *afp4b* transcript are respectively indicated by red or blue boxes; targets of tb-MOs are pointed out by brackets.

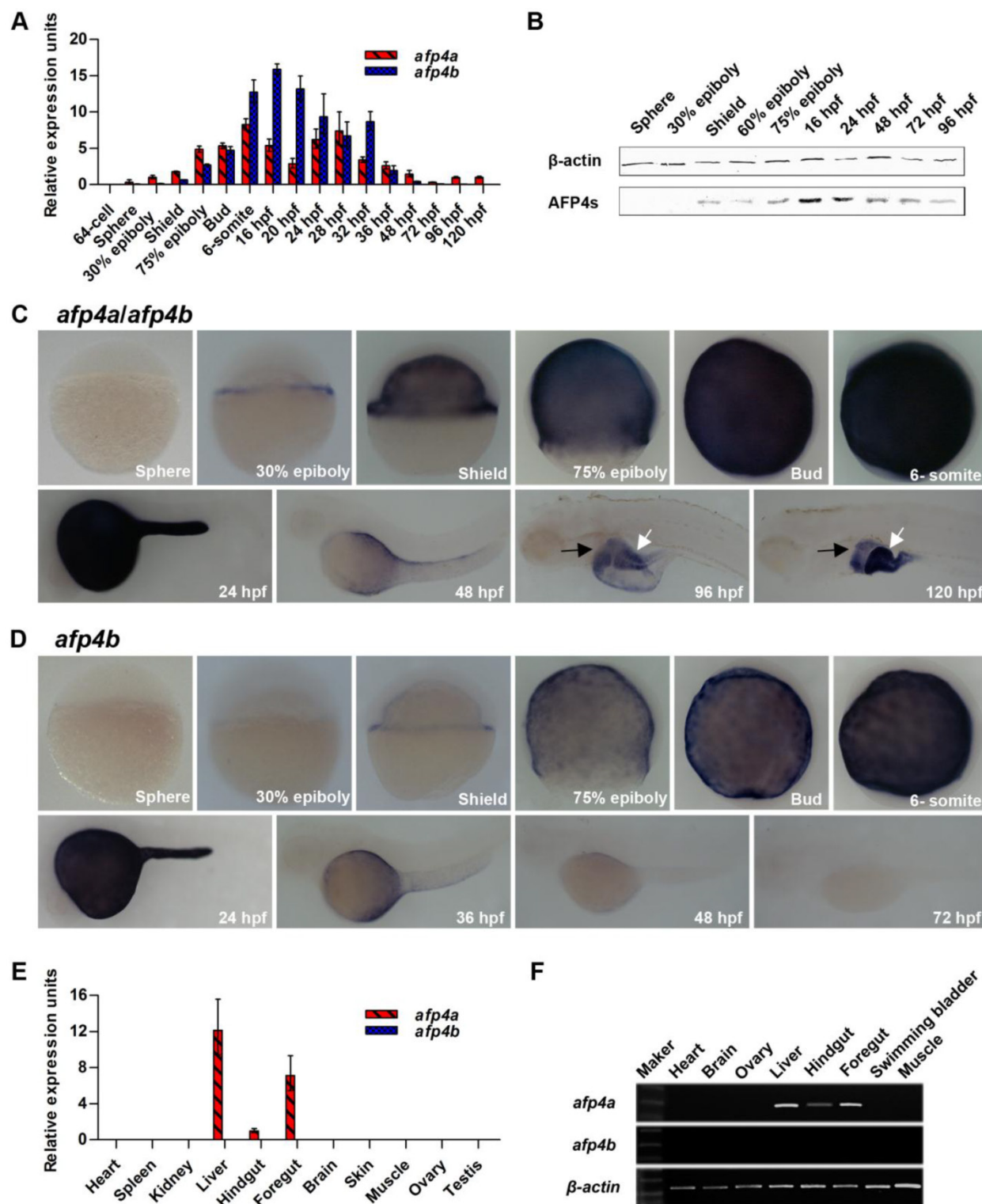


Figure 2. Temporal and spatial expression pattern of *afp4s*. (A) Expression of *afp4a* and *afp4b* in embryonic development stages and early larvae evaluated by qPCR and normalized to β -actin. The histograms stand for the relative transcript level of *afp4a* (red) or *afp4b* (blue), and the relative transcript level of *afp4a* at the sphere stage is set to 1. Data shown are means \pm SD of three independent assays. (B) Western blot assay from sphere stage to 96 hpf. β -actin protein is internal control. (C, D) *In situ* hybridized WT embryos for *afp4a/afp4b* (C) or *afp4b* (D). Stages of embryos are shown in the bottom right corner of each panel. Black arrows indicate the liver, and white arrows indicate the intestine. Embryos from sphere stage to 6-somite stage are oriented animal pole up and dorsal right, and embryos from 24 hpf to 120 hpf are heading to the left and dorsal up. (E, F) Expression of *afp4a* and *afp4b* in adult tissues evaluated by qPCR (E) and semi-quantitative RT-PCR (F), and normalized to β -actin. (E) The histograms stand for the relative transcript level of *afp4a* (red) or *afp4b* (blue), and the relative transcript level of *afp4a* in the hindgut is set to 1. Data shown are means \pm SD of three independent assays.

Yolk syncytial layer and digestive system-specific expression of *afp4s* in embryos, early larvae, and adults

Moreover, the expression patterns of *afp4a* and *afp4b* were investigated in embryos and larvae by WISH using two different antisense probes. The first probe, targeted to a 5'-terminal 506 nt sequence of *afp4a* transcript (Fig. 1C), can recognize both transcripts of *afp4a* and *afp4b* because of their high sequence similarity. The second probe, which is mainly against to extra 3'-terminal of *afp4b* with 553 nt (Fig. 1C), is only able to examine the *afp4b* transcript. These WISH data further revealed a differential and dynamic expression fashion between *afp4a* and *afp4b*. As shown in Fig. 2C, the positive signal hybridized with the first probe initiates to appear in YSL from 30% epiboly stage at about 4.7 hpf. Then, the signal quickly enhances from shield stage at about 6 hpf, and reaches to the strongest from 8 hpf to 12 hpf during which 75% epiboly, tail-bud formation and somitogenesis (6-somite) have progressed. The sectioned observations of the stained embryos from shield to bud stages showed restricted expression in YSL (Supplementary material Fig. S2A-C). Along with the embryonic development, the specific expression domain in YSL becomes clearer, especially in 24 hpf embryos. After yolk absorption, the signal gradually becomes weak from the posterior to anterior YSL in the hatched larvae, and finally restricts to the formed digestive organs, including intestine and liver, in 96 hpf and 120 hpf larvae. In comparison with the above data, the *afp4b*-specific transcript expresses later, and also appears within YSL from the shield stage embryos at about 6 hpf. Then, its expression strengthens rapidly, and reaches the strongest at about 12 hpf when the embryos develop to 6-somite stage (Fig. 2D). The longitudinal section of the stained embryos also showed specific expression in YSL (Supplementary material Fig. S2D-F). After 24 hpf, the *afp4b*-specific transcript reduces gradually, and not any *afp4b*-specific transcript is observed in the corresponding expression position after 72 hpf (Fig. 2D).

Furthermore, tissue distribution of *afp4a* and *afp4b* transcripts was examined in adult zebrafish by qPCR and semi-quantitative RT-PCR. As shown in Fig. 2E and 2F, the *afp4a* transcript is abundant in liver and foregut, slight in hindgut, and no signal exists in other tissues, including heart, spleen, kidney, brain, skin, muscle, ovary, testis and swimming bladder, whereas *afp4b* mRNA is absent in all the examined tissues. All the data indicate that both transcripts of *afp4a* and *afp4b* express specifically in YSL, but the later expressed *afp4b* appears only in embryogenesis, whereas *afp4a* expresses continually in YSL and di-

gestive system from early embryos to adults, suggesting that *afp4a* and *afp4b* might play similar but different biological roles during zebrafish embryogenesis and early larval development.

AFP4a and AFP4b contribute to early morphogenetic movements during zebrafish embryogenesis

To explore their respective biological functions, we designed two kinds of antisense MOs specific to *afp4a* or *afp4b*. One is translation-blocking MO (tb-MO), which is directed to the 5' UTR of *afp4a* (*afp4a*-tb-MO) or *afp4b* (*afp4b*-tb-MO) (Fig. 1C). The efficiency and specificity of each tb-MO were confirmed by co-injecting with *afp4a*:EGFP or *afp4b*:EGFP mRNA (100 pg/embryo) into one-cell stage zebrafish embryos. The test showed that about 8 ng *afp4a*-tb-MO for each embryo could largely deplete the EGFP fluorescence produced by *afp4a*:EGFP mRNA, but did not inhibit that expressed by *afp4b*:EGFP mRNA. On the other hand, lower dose *afp4b*-tb-MO (2.5 ng/embryo) could completely deplete the EGFP fluorescence produced by *afp4b*:EGFP mRNA, but did not reduce that produced by *afp4a*:EGFP mRNA. However, if the dose of *afp4b*-tb-MO was increased to 5 ng, the proportion of *afp4a*:EGFP-injected embryos with EGFP fluorescence was significantly reduced to 62% (Supplementary material Fig. S3A). These data indicate that *afp4a*-tb-MO can specifically knockdown AFP4a expression, whereas *afp4b*-tb-MO can specifically deplete AFP4b expression only at a lower dose, and a higher dose can interfere with the specificity and lead to cross-reaction with *afp4a*.

The other kind of MO is splice-blocking morpholino (sb-MO), which is targeted to the intron 3/exon 4 boundary of *afp4a* (*afp4a*-sb-MO) or *afp4b* (*afp4b*-sb-MO), since significant nucleotide difference only exists in the boundary sequence between *afp4a* and *afp4b* premature mRNAs (Supplementary material Table S2). The sb-MO resulted in a transcript with intron 3 insertion, and introduced a premature stop codon right after the exon 3/intron 3 junction. This early stop codon led to a truncated protein (58 amino acid residues), which lost the entire product of exon 4, including the characteristic 11-mer conserved repeats in all AFP4s (Fig. 1B, Supplementary material Fig. S3B and Table S2). Semi-quantitative RT-PCR results showed that 4 ng *afp4a*-sb-MO could specifically change the splice of all the endogenous *afp4a* mRNA, while 8 ng *afp4b*-sb-MO could only specifically change the splice of about half the endogenous *afp4b* mRNA (Supplementary material Fig. S3B).

Then, 4 MOs were respectively injected with appropriate concentration described above. When

Ctrl-MO (8 ng/embryo) embryos developed to bud stage, both *afp4a-tb*-MO (8 ng/embryo) morphants and *afp4a-sb*-MO (4 ng/embryo) morphants displayed an epibolic delay; nevertheless, a more serious defect in epiboly was observed in *afp4a-sb*-MO morphants. At the same time, both *afp4b-tb*-MO (2.5 ng/embryo) morphants and *afp4b-sb*-MO (8 ng/embryo) morphants showed a longer anterior-posterior axis, and *afp4b-sb*-MO led to a similar but milder defect (Supplementary material Fig. S3C). The two distinct MOs targeted to the same gene caused the similar defect, confirming the phenotypes-specific to *afp4a* or *afp4b*. Moreover, *afp4a-sb*-MO and *afp4b-tb*-MO could produce the more obvious defect with lower individual MO dose than the other MO targeted to the same gene, and the lower dose was likely to cause fewer non-specific defects. Therefore, *afp4a-sb*-MO and *afp4b-tb*-MO were used in subsequent experiments.

Subsequently, *afp4a-sb*-MO (4 ng/embryo) and *afp4b-tb*-MO (2.5 ng/embryo) were respectively or simultaneously (*afp4*-MOs) injected into zebrafish embryos at the one-cell stage. Western blot detection further confirmed the specificity and effectiveness. A significant decrease of AFP4s level was observed from shield stage (about 92% reduction) to 6-somite stage (about 64% reduction) in the *afp4a-sb*-MO morphants, whereas a contrary change was detected from shield stage (about 6% reduction) to 6-somite stage (about 38% reduction) in the *afp4b-tb*-MO morphants (Fig. 3A and 3B). These are consistent with the higher transcript level of *afp4a* than that of *afp4b* before 6-somite stage. Significantly, all the AFP4s were completely depleted from shield stage to 6-somite stage in the *afp4a-sb*-MO and *afp4b-tb*-MO co-injected (*afp4*-MOs) morphants.

Moreover, morphologic changes of embryos in each group were closely monitored. When Ctrl-MO embryos developed to shield stage, at which time their blastoderm covered 50% of the yolk and formed shield, *afp4a-sb*-MO morphants also formed shield, but their blastoderm could not cover half of the yolk. While Ctrl-MO embryos reached 75% epiboly, *afp4a-sb*-MO morphants displayed an obvious delay in epiboly. At the bud stage, when epiboly was completed in Ctrl-MO embryos, about 20% yolk could not be covered by blastomeres in *afp4a-sb*-MO morphants (Fig. 3C, D). Significantly, the *afp4b-tb*-MO injected embryos did not show any obvious defects until 75% epiboly, but the morphants began to display a longer anterior-posterior axis from bud stage. Moreover, delayed developments were observed during somitogenesis, in which their somites became wider in the mediolateral axis and the boundary of somites was

faint. At 24 hpf, the *afp4b-tb*-MO injected embryos displayed shorter anterior-posterior body axis without distinct v-shape somites, and approximately 49.3% of the morphants died (Fig. 3E, G). In contrast, the *afp4a-sb*-MO injected embryos showed a more normal phenotype than the *afp4b-tb*-MO morphants after bud stage. At 6-somite stage, about 85.4% morphants, which had closed their blastopores, showed a slight increased linear distance between the head and tail, and about 8.0% morphants still could not finish epiboly (data not shown). However, some obvious defects, such as curving trunk, reduction of yolk extension and diminution of head growth, were observed at 24 hpf. Meanwhile, the 8.0% *afp4a-sb*-MO morphants, which failed to finish epiboly, displayed a curly tail (Fig. 3D). In comparison with the *afp4a-sb*-MO (Fig. 3D) or *afp4b-tb*-MO (Fig. 3E) morphants, the morphogenetic defects during gastrulation (from shield stage to bud stage) in the *afp4*-MOs co-injected morphants (Fig. 3F) were basically similar to that in the embryos merely injected with *afp4a-sb*-MO (Fig. 3D). However, the proportion of the dead *afp4*-MOs embryos was higher (about 33.3%) than that of the embryos only injected with *afp4a-sb*-MO (about 2.4%) or *afp4b-tb*-MO (about 2.5%) at bud stage (Fig. 3G). Two hours later, when embryos developed to 6-somite stage, the survived *afp4*-MOs morphants showed the delayed development of head, elongated anterior-posterior axis and faint somite boundary, or even crooked notochord. Furthermore, the proportion of dead *afp4*-MOs-injected embryos increased substantially to approximately 83.1%, whereas those of single MO injected embryos were still very low (about 3.5% for *afp4a-sb*-MO, and 3.9% for *afp4b-tb*-MO). At 24 hpf, the survived *afp4*-MOs morphants showed similar phenotypes with *afp4b-tb*-MO morphants, and the proportion of dead embryos increased to about 86.8%. (Fig. 3F, G)

To confirm the specificity for above data, we synthesized mRNA of *afp4a* and *afp4b* lacking 5' UTR, where was the target of tb-MO for rescue examination. Remarkably, the morphogenetic defects caused by the *afp4*-MOs could be rescued by the synthesized mRNA of *afp4a* and *afp4b*, because significant death decrease and significant wild type increase appeared in the co-injected embryos of each or mixture of *afp4a*-mRNA and *afp4b*-mRNA ($P < 0.001$). However, phenotype and death were still at high levels. (Fig. 3G) This observation could because that the RNA amount injected to embryos was not most suitable for rescue. These data suggest that AFP4a and AFP4b might contribute to early morphogenetic movements during zebrafish embryogenesis.

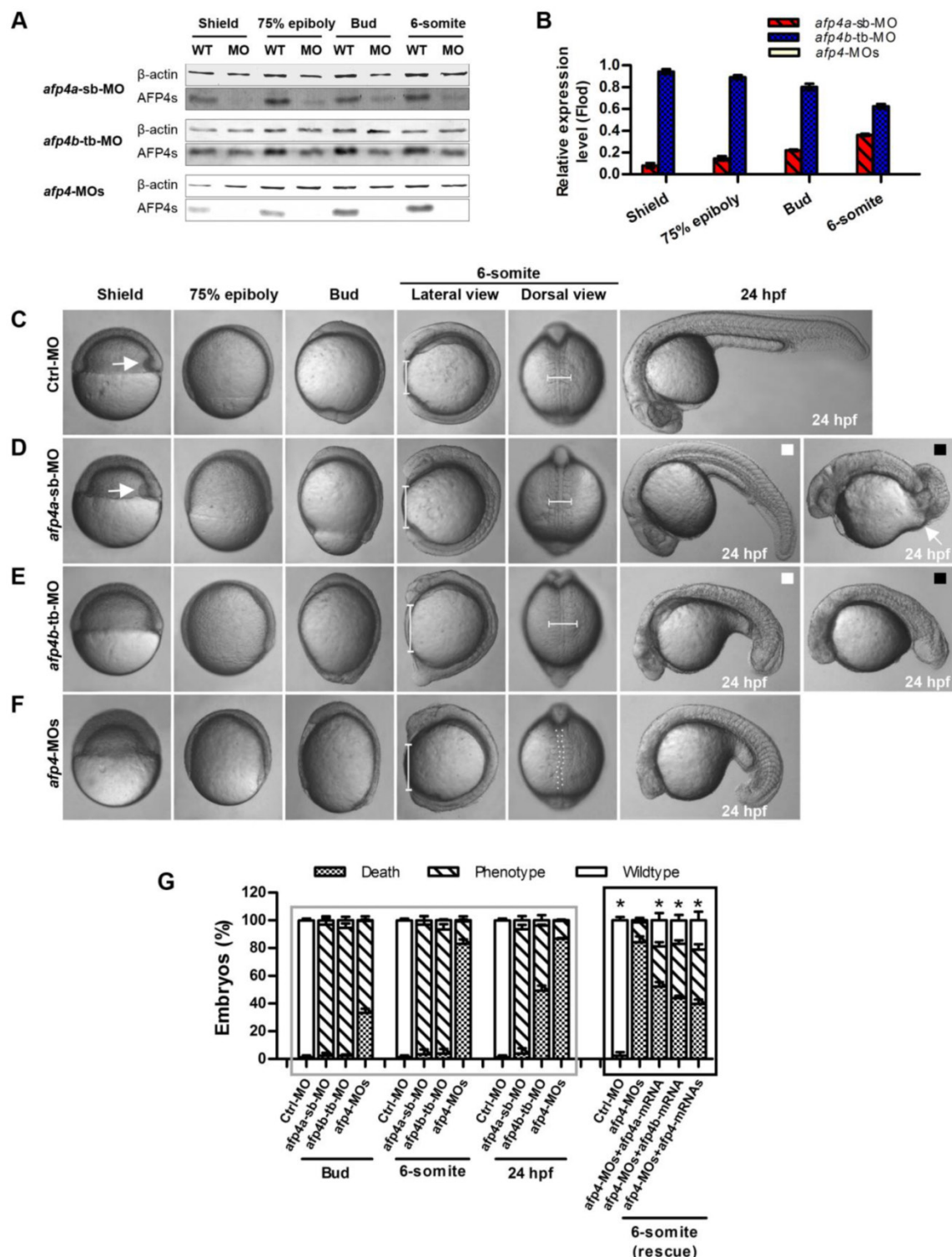


Figure 3. Reduced AFP4a and/or AFP4b expression causes serious morphogenetic defects during early embryonic development. (A) Test of decrease of AFP4s by Western blotting at shield stage, 75% epiboly stage, bud stage and 6-somite stage after injection of *afp4a-sb-MO* and/or *afp4b-tb-MO*. *afp4-MOs* means *afp4a-sb-MO* and *afp4b-tb-MO* co-injection. β-actin protein is internal control. (B) Statistical data of the relative AFP4s expression level in *afp4a-sb-MO* and/or *afp4b-tb-MO* morphants from shield stage to 6-somite stage. Normalized to the expression of β-actin protein and the corresponding relative expression level of AFP4s in WT embryos is set to 1. Results are presented as means ± SD of three independent experiments. (C-F) Morphology of embryos from shield stage to 24 hpf after injecting Ctrl-MO (C), *afp4a-sb-MO* (D), *afp4b-tb-MO* (E), or *afp4-MOs* (F). Lateral views of embryos from shield to bud stage, dorsal to the right, anterior at the top; lateral or dorsal views of embryos at 6-somite stage with their animal pole facing upward; lateral views of embryos at 24 hpf, anterior towards the left and dorsal to the top. The arrows in shield stage embryos indicate the shield; the arrow in 24 hpf *afp4a-sb-MO* morphants indicates the unclosed blastopore; the lines in lateral-viewed 6-somite stage embryos indicate head-to-tail distance; the lines in dorsal-viewed embryos indicate somites width; the dotted lines show the boundary of a curve notochord. Morphology was scored as mild (white) or severely defective (black) in *afp4a-sb-MO* or *afp4b-tb-MO* injected embryos at 24 hpf. (G) Percentage of embryos at bud stage, 6-somite stage and 24 hpf in each class after injecting Ctrl-MO, *afp4a-sb-MO*, *afp4b-tb-MO*, or *afp4-MOs* (the left columns indicate by a grey box). Results represent means ± SD of three independent experiments, N=76 to 116 embryos per condition; or percentage of *afp4-MOs*-injected embryos in each class at 6-somite stage after injecting *afp4a-mRNA*, *afp4b-mRNA*, or *afp4a-mRNA* together with *afp4b-mRNA* (*afp4-mRNAs*) (the right columns indicate by a black box). Results represent means ± SD of three independent experiments, N=55 to 89 embryos per condition. * means P < 0.001, when compared to *afp4-MOs*.

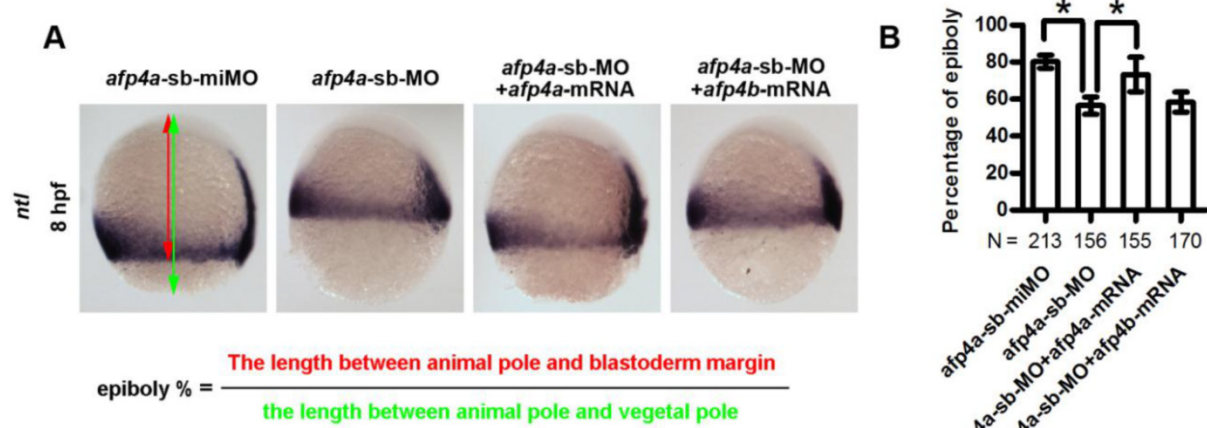


Figure 4. The reduced AFP4a expression leads to epibolic delay. (A) *ntl* expression in 8 hpf groups injected with *afp4a-sb-miMO*, *afp4a-sb-MO*, *afp4a-sb-MO* plus *afp4a-mRNA*, or *afp4a-sb-MO* plus *afp4b-mRNA*. Lateral views of embryos, dorsal to the right, anterior to the top. The calculating method for the epiboly percentage is shown. (B) Histogram represents mean \pm SD of the epiboly percentage in each group. N, the number of embryos that were analyzed from three independent experiments. *P < 0.01.

AFP4a is required for epiboly progression

To confirm whether the morphogenetic defect in the *afp4a-sb-MO* morphants during gastrulation was resulted from AFP4a depletion, we further synthesized a control MO containing 5-base mismatches relative to *afp4a-sb-MO* (*afp4a-sb-miMO*). Identically to the above Ctrl-MO, the embryos injected with 4 ng of *afp4a-sb-miMO* were normal, and thus the *afp4a-sb-miMO* was utilized as a control in following studies on the role of AFP4a. In addition, the synthesized *afp4a* or *afp4b* mRNA was co-injected with *afp4a-sb-MO* for rescue examination, and the mesodermal marker *ntl* was used to visualize the blastoderm margin through WISH (Fig. 4A) and thereby to quantify the epiboly percentage (Fig. 4B). In comparison with normal epiboly progression (80.2% \pm 3.7%, N=213) at 8 hpf in the *afp4a-sb-miMO* embryos, the *afp4a-sb-MO* embryos displayed significant epiboly delay (56.5% \pm 5.0%, N=156), and the delay could be rescued by co-injection with 150 pg *afp4a-mRNA* (73.1% \pm 9.3%, N=155), but could not be restored by the same amount of *afp4b-mRNA* (58.3% \pm 6.1%, N=170). These data indicate that AFP4a depletion leads to epiboly defect.

Since the *afp4a*-expressed YSL had been revealed to play significant roles in germ layer differentiation and early morphogenetic movements [46], we further tested whether the AFP4a depletion affected other early embryonic development except for epiboly progression. Firstly, we detected germ layer differentiation by endodermal marker *foxA3*, mesendodermal marker *gsc* and mesodermal marker *ntl* in shield stage embryos. In comparison with the *afp4a-sb-miMO* control embryos, their expression domains at the gastrulation onset stage were only located slightly towards animal-pole in the *afp4a-sb-MO* morphants (Supplementary material Fig. S4A-C). These changes

should be caused by epiboly delay, and germ layer differentiation is little affected in the AFP4a-knockdown embryos. At the same stage, AFP4a-depleted embryos also showed the prominent embryonic shield similar to that in control embryos, even though the blastoderms in these embryos covered less than 50% of the yolk cell (Fig. 3D). This phenotype implies that involution movement is normal in the morphants.

Moreover, localization of *ntl* in axial chordal mesoderm and *myoD* in adaxial cells at bud stage confirmed the presence of a slight wider and shorter axis with the unclosed blastopore in *afp4a-sb-MO* morphants (Supplementary material Fig. S4D and E), but the expression domains of *myoD* in adaxial cells and somites were comparable between *afp4a-sb-MO* morphants and *afp4a-sb-miMO* morphants at 8-somite stage when most *afp4a-sb-MO* morphants finished epiboly (Supplementary material Fig. S4F). These data indicate that mediolateral convergence seems a little change because of the unclosed blastopore. On the other hand, the normality in anterior part of *ntl* expression domain was observed (Supplementary material Fig. S4G). Moreover, the expression of *hgg1*, which marked the prechordal plate, and of *dlx3b*, which expressed in the anterior edge of the neural plate, were almost the same as *afp4a-sb-miMO* embryos at the bud stage (Supplementary material Fig. S4H). In addition, at the 8-somite stage, the expression domains of *pax2.1* in the optic stalk, the midbrain/hindbrain boundary, and the otic vesicles were comparable between *afp4a-sb-MO* morphants and *afp4a-sb-miMO* morphants (Supplementary material Fig. S4I). These data indicate that the anterior extension of the axial mesendoderm is not affected, and the convergence movement is slightly affected by AFP4a deficiency.

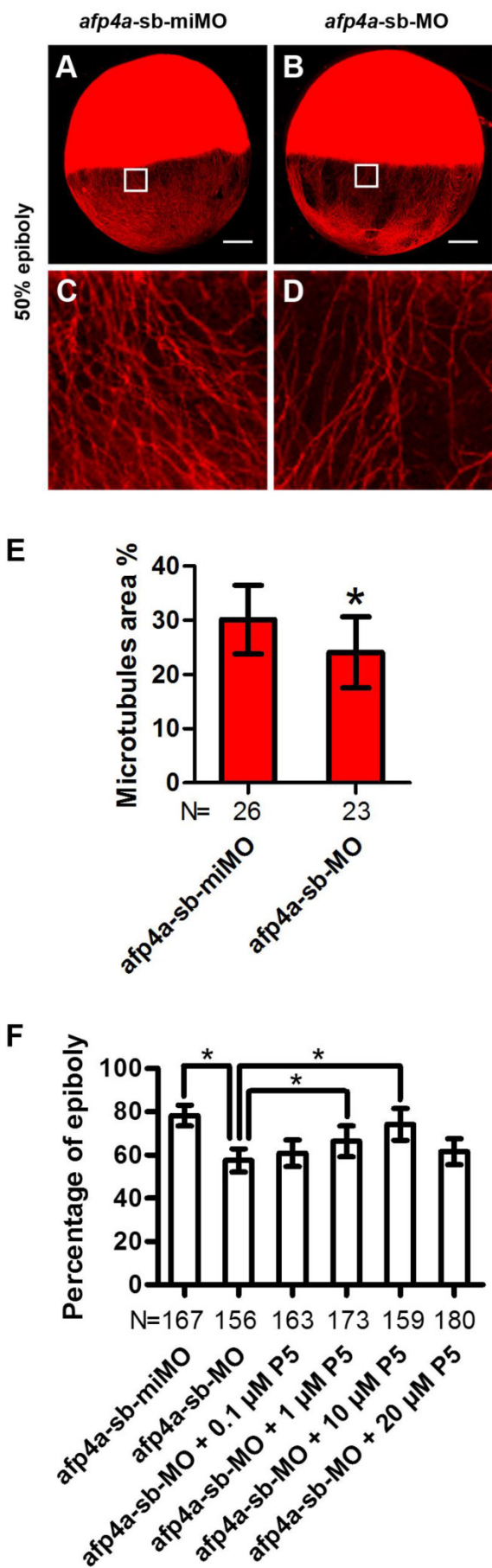


Figure 5. YCL microtubule arrays of *afp4a-sb-MO* morphants are less stable than that of *afp4a-sb-miMO* control embryos. (A-D) YCL microtubules are thinner in *afp4a-sb-MO* embryos (B, D) compared to those in *afp4a-sb-miMO* embryos (A, C), at 50% epiboly after nocodazole treatment. (C or D) is the enlarged image of the areas in the square in (A or B). Embryos are oriented with anterior up. Scale bars, 100 μ m. (E) Average percentage of the microtubule area in YCL alone EVL margin in *afp4a-sb-miMO* embryos and *afp4a-sb-MO* morphants at about 50% epiboly after nocodazole treatment. (F) Epibolic defect in AFP4a-deficient embryos can be rescued by 1 and 10 μ M pregnenolone (P5). (E and F) Data are represented as means \pm SD. N, the number of embryos that were analyzed from three independent experiments. * $P < 0.01$.

AFP4a participates in epiboly progression by stabilizing YCL microtubules

Above observed phenotypes in the *afp4a-sb-MO* morphants, such as obviously delayed epiboly, mildly affected CE, and normal germ layer induction, involution and anterior axial formation, are highly similar to those of YCL microtubule disrupted embryos [6, 47]. This strong resemblance promoted us to visualize microtubule array in YCL by staining them with antibody against β -tubulin. Firstly, we compared the *afp4a-sb-miMO* and *afp4a-sb-MO* embryos fixed at 50% epiboly stage, and no any changes were observed (data not shown). Then, we treated the *afp4a-sb-miMO* and *afp4a-sb-MO* embryos at 50% epiboly stage with 1 μ g/ml nocodazole for 20 min at 28.5°C, and examined the microtubules again in the fixed embryos. Obviously, the YCL microtubules in the *afp4a-sb-MO* embryos were thinner than those in the *afp4a-sb-miMO* embryos (Fig. 5A-D). To quantify the data, the percentages of microtubule area in 100 \times 100 pixel images were obtained, and a statistical analysis was performed. The average percentage of microtubule area was 30.1% ($SD=6.3\%$, $N=26$) in the *afp4a-sb-miMO* embryos, whereas it was only 24.1% ($SD=6.6\%$, $N=23$) in the *afp4a-sb-MO* morphants (Fig. 5E), indicating that the stability of microtubules is reduced in the *afp4a-sb-MO* morphants.

To confirm that the epiboly delay resulted from the microtubule disruption, we used pregnenolone (P5, 0.1, 1, 10 and 20 μ M) to incubate the *afp4a-sb-MO* morphants, since pregnenolone was demonstrated to promote epiboly by stabilizing microtubules [6]. Significantly, when *afp4a-sb-miMO* embryos reached to 78.2% epiboly ($SD=4.8\%$, $N=167$), the blastoderms only covered 57.4% yolk cells ($SD=5.4\%$, $N=156$) in the *afp4a-sb-MO* morphants. In addition, the epibolic defect of *afp4a-sb-MO* morphants could be partially rescued by the pregnenolone treatment, in which the significant rescuing increases were observed from 1 to 10 μ M pregnenolone treatment ($66.3\% \pm 7.2\%$, $N=173$; $74.1\% \pm 7.3\%$, $N=159$). However, a rescuing decrease was observed in 20 μ M treatment ($61.4\% \pm 6.0\%$, $N=180$) (Fig. 5F). A similar epibolic defect was also observed in embryos treated by high dose of microtubule stabilizing agent taxol [48]. In this respect, this

decrease could be interpreted as a result of too stable microtubule arrays. These results indicate that YCL microtubule cytoskeleton is disturbed in the *afp4a* morphants, suggesting that AFP4a might participate in epiboly progression by stabilizing YCL microtubules.

Another actin cytoskeleton structure, including F-actin rings at the vegetal margin of deep cells and EVL, and punctuate actin band in the external-YSL lying vegetal to the EVL leading margin, which form after 50% epiboly, had been revealed to be an important drive of the second half epiboly [43]. To reveal whether the actin cytoskeleton was also affected in the *afp4a* morphants, we performed F-actin staining with rhodamine-phalloidin. In *afp4a*-sb-miMO embryos, the punctuate actin band initiated to form at 6 hpf and

became very clear at 7 hpf (Fig. 6A, C and E), whereas in the *afp4a*-sb-MO morphants, it began to appear at 7 hpf and displayed obviously at 8 hpf (Fig. 6B, D and F). This difference might be resulted from epiboly progression delay. Quantitative analyses indicated that there were obviously different phalloidin signals between the *afp4a*-sb-miMO embryos and the *afp4a* morphants at their corresponding 6 hpf and 7 hpf (Fig. 6G, H), but basic similar phalloidin intensity signals were observed from their same development stages, when 50% or 60% epiboly embryos were comparatively analyzed (Fig. 6I). The results suggest that the actin cytoskeleton should be not affected in the *afp4a* morphants, and AFP4a might specifically interact with YCL microtubules to participate in epiboly progression.

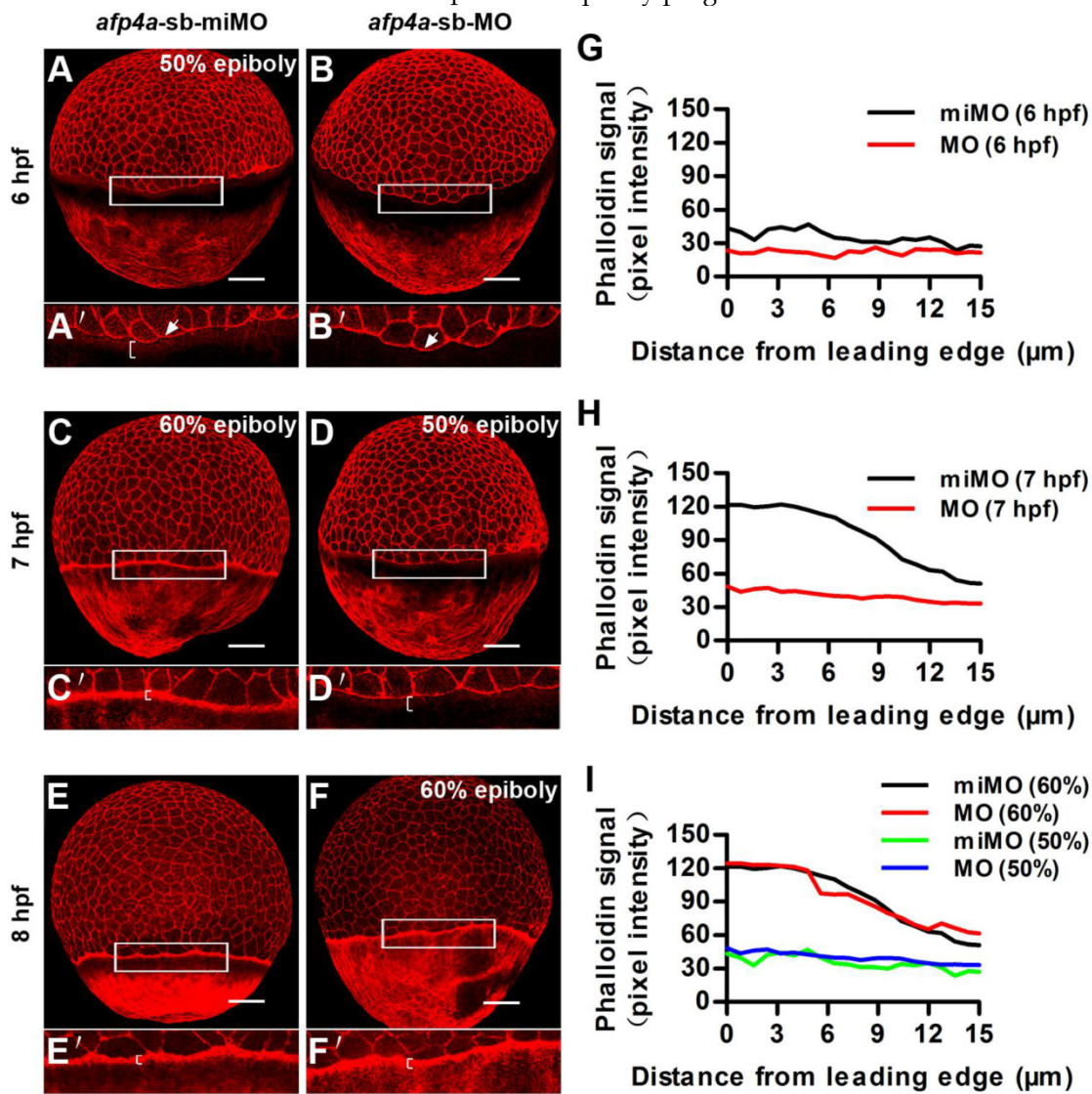


Figure 6. Formation of the punctate actin band in YSL seems to be timed by an epiboly-dependent clock in *afp4a*-sb-MO morphants. (A-F) *afp4a*-sb-miMO embryos (A, C, E) and the same-age *afp4a*-sb-MO embryos (B, D, F) at 6 hpf (A, B), 7 hpf (C, D) and 8 hpf (E, F) stained with rhodamine-phalloidin (F-actin). Among them, *afp4a*-sb-miMO morphants at 6 hpf (A) and *afp4a*-sb-MO morphants at 7 hpf (D) reach about 50% epiboly, and *afp4a*-sb-miMO morphants at 7 hpf (C) and *afp4a*-sb-MO morphants at 8 hpf (F) reach about 60% epiboly. (A'-F') are the enlarged images of the areas in the rectangle in corresponding (A-F). Embryos are oriented with their animal pole up; brackets in A'-F' indicate the punctuate actin bands; white arrows in A' and B' indicate leading edge of the EVL; scale bars, 100 μm . (G-I) Average intensity of phalloidin signal in the YSL along the EVL margin in *afp4a*-sb-miMO (miMO) embryos and *afp4a*-sb-MO (MO) morphants at 6 hpf (G), 7 hpf (H) and 50% and 60% epiboly (I). The intensity of the phalloidin signal was plotted along a line perpendicular to the EVL margin. Average plots of ten embryos for each group are shown.

AFP4b is required for CE movement without affecting dorsoventral axis patterning

To investigate the role of AFP4b in embryogenesis, we synthesized a 5-base mismatched control MO to *afp4b-tb-MO* (*afp4b-tb-miMO*), and observed a normal embryo phenotype similar to the Ctrl-MO injection at same concentration of 2.5 ng/embryo (data not shown). So, the *afp4b-tb-miMO* was served as a control of the *afp4b-tb-MO* in subsequent research about the function of AFP4b. In comparison with control *afp4b-tb-miMO* embryos, the somite width was significantly enhanced in the *afp4b-tb-MO* morphants at 8-somite stage, as revealed by *myoD* probe. This abnormality could be rescued only by co-injection of 150 pg *afp4b*-mRNA, but not by the same amount of *afp4a*-mRNA (Fig. 7A). A quantitative and statistical analysis showed a significant increase of average somite width ($251.4 \pm 45.2 \mu\text{m}$, N=176, P < 0.01) in the *afp4b-tb-MO* morphants relative to that in the

afp4b-tb-miMO embryos ($192.0 \pm 10.3 \mu\text{m}$, N=160). Moreover, this increase could be effectively recovered by the *afp4b*-mRNA co-injection ($195.6 \pm 40.1 \mu\text{m}$, N=149), but could not be rescued by the same amount of *afp4a*-mRNA ($245.6 \pm 37.6 \mu\text{m}$, N=153) (Fig. 7B). These data indicate that the somite defect is resulted from specific reduction of AFP4b expression.

The above somite defect implied that AFP4b might be involved in CE movements, because it was very similar to the previous observation in *has2* and *rhoA* morphants [49, 50]. For this reason, we firstly used dorsal (*gsc*) and ventral (*evel*) makers to detect dorsoventral patterning change in the *afp4b-tb-MO* morphants. In comparison with *afp4b-tb-miMO* embryos, no any obvious change was observed in the *afp4b-tb-MO* morphants at 75% epiboly (Fig. 7C, D), indicating that AFP4b knockdown did not disrupt dorsoventral axis patterning and differentiation.

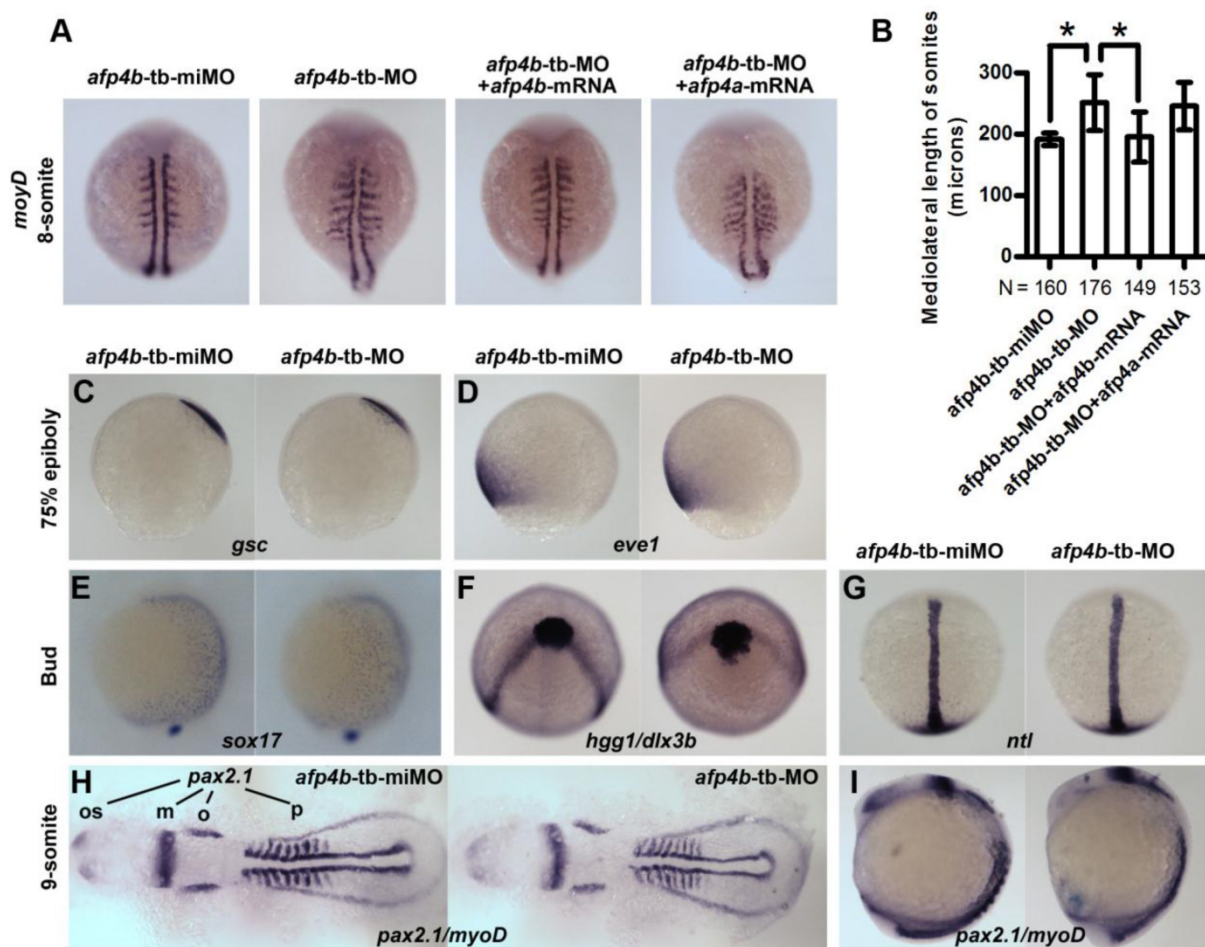


Figure 7. Reduced AFP4b expression affects CE movement. (A) *myoD* expression in 8-somite groups injected with *afp4b-tb-miMO*, *afp4b-tb-MO*, *afp4b-tb-MO* plus *afp4b*-mRNA, or *afp4b-tb-MO* plus *afp4a*-mRNA. Dorsal views of embryos, anterior to the top. (B) Average mediolateral length of somites in each group. Error bars show SD. N, the number of embryos that were analyzed from three independent experiments. *P < 0.01. (C-I) Dorsoventral pattern is normal, but CE is affected in *afp4b-tb-MOs* morphants showing by whole-mount *in situ* hybridization. In each section, expression of marker genes in *afp4b-tb-miMO* morphants (left) and *afp4b-tb-MO* morphants (right) are shown. (C) *gsc*, 75% epiboly stage. (D) *evel*, 75% epiboly stage. (E) *sox17*, bud stage. (C-E) Lateral views, dorsal to the right. (F) *hgg1* and *dlx3b*, bud stage, top view, ventral up. (G) *ntl*, bud stage, dorsal view, animal pole to the top. (H and I) *pax2.1* and *myoD*, 9-somite stage. (H) Flat-mounted embryos, head to the left. os, optic stalk; m, the midbrain hindbrain boundary; o, otic vesicles; p, pronephros. (I) Lateral view, dorsal to the right.

Moreover, we detected CE movements by marker genes specific to endoderm (*sox17*), axial and paraxial mesoderm (*hgg1*, *ntl*, *myoD*), and neuroectoderm (*dlx3b* and *pax2.1*). The *sox17*-labeled endoderm cells moved slower dorsally during gastrulation in *afp4b-tb-MO* morphants, as indicated by the earlier dorsoventral expression pattern of *sox17* at the end of gastrulation (Fig. 7E). Thus, the CE defect in *afp4b-tb-MO* morphants might be associated with dorsal migration of ventrolateral endoderm cells. In addition, the neural plate was much wider in *afp4b-tb-MO* morphants, as reflected by the laterally expansion expression domain of *dlx3b* at bud stage (Fig. 7F) and *pax2.1* (the midbrain hindbrain boundary, the otic vesicles) at 9-somite stage (Fig. 7H). Thus, the CE movement of neuroectoderm was delayed in *afp4b-tb-MO* morphants. Moreover, *afp4b-tb-MO* morphants showed indistinguishable notochord from control embryos, as revealed by the expression of *ntl* at bud stage (Fig. 7G). However, *afp4b* morphants displayed a broader somatic mesoderm and short head to tail distance during somitogenesis, as represented by the expression patterns of *myoD* and *pax2.1* (the optic stalk to the posterior end of the pronephros) in Flat-mounted embryos at 9-somite stage (Fig. 7H). At the same time, *afp4b-tb-MO* morphants still showed a longer anterior-posterior axis (Fig. 7I). Similar observations were also reported in research of *has2* and *npc1* [7, 49]. Therefore, the CE movement of axial mesoderm was least affected, but that of paraxial

mesoderm was significantly changed in *afp4b-tb-MO* morphants. The above data indicate that CE movement of ventrolateral cells is severely impaired, whereas CE movement of axial cells and dorsoventral axis patterning are normal after the AFP4b knockdown, implying that AFP4b is required for CE movement without affecting dorsoventral axis patterning.

AFP4b is primarily related to convergence

To directly clarify how CE movements are affected by AFP4b depletion during gastrulation, we respectively injected Kaede mRNA with *afp4b-tb-miMO* or *afp4b-tb-MO* into one-cell stage embryos. Then, Kaede protein was activated from green to a bright and stable red fluorescence by UV illumination at a specific time and in a specific cell group, and cell movements were traced as previously described [41]. Firstly, the lateral marginal cells, 90° from the dorsal shield, were activated at 6 hpf by a focused UV pulse (Fig. 8A and D), and the movement trajectories of the labeled red fluorescence cells were traced. In comparison with normal movement trajectories in *afp4b-tb-miMO* embryos (Fig. 8B and C), the labeled red fluorescence cells in the *afp4b-tb-MO* embryos underwent normal animal and vegetal migrations, but the movement towards the dorsal side was severely affected, and the labeled cells did not reach to the midline (Fig. 8E and F).

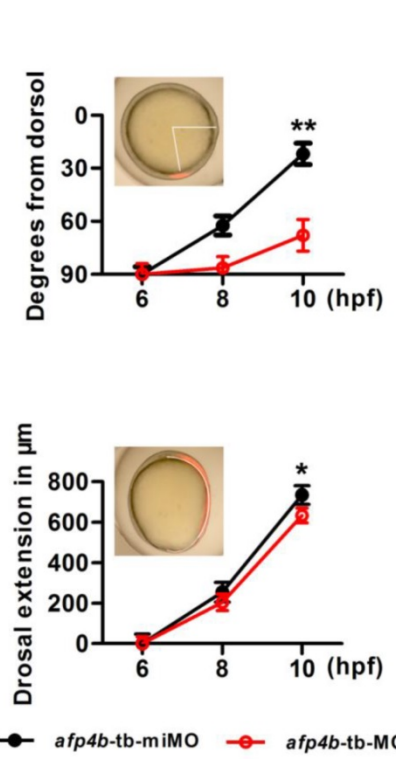
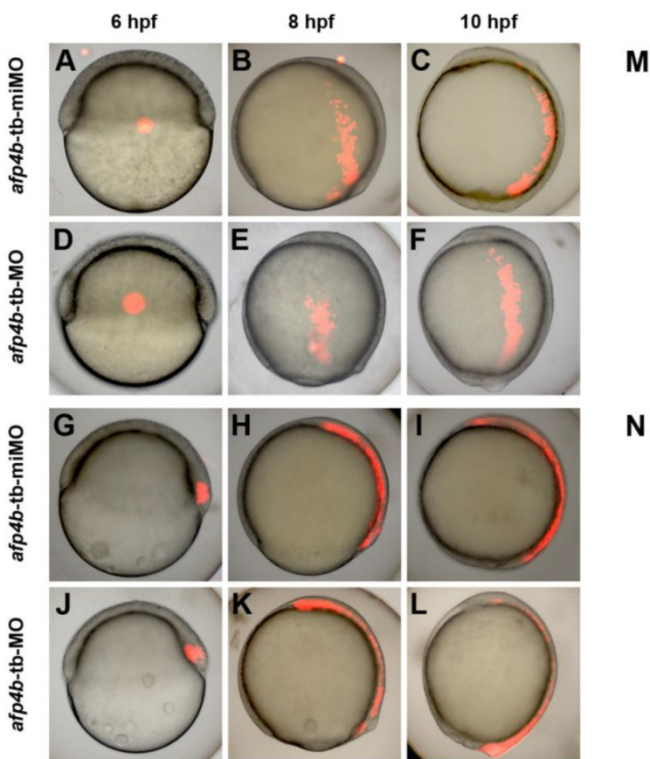


Figure 8. Cell tracing experiments. (A-F) Distribution of labeled lateral cells in *afp4b-tb-miMO* embryos (A-C) and *afp4b-tb-MO* embryos (D-F) at 6 hpf (A, D), 8 hpf (B, E) and 10 hpf (C, F). (G-L) Distribution of labeled dorsal cells in *afp4b-tb-miMO* embryos (G-I) and *afp4b-tb-MO* embryo (J-L) at 6 hpf (G, J), 8 hpf (H, K) and 10 hpf (I, L). (M) Lateral views, animal pole is up and dorsal is to the right. (N) Graph displaying the average degree from the dorsal axis to labeled cells (indicated by angle) at 6 hpf, 8 hpf and 10 hpf, **P < 0.001. (N) Graph displaying the average extension in labeled dorsal cells (indicated by arc) at 6 hpf, 8 hpf and 10 hpf, *P < 0.05. Ten embryos per treatment were evaluated, and error bars show SD.

A quantitative and statistical analysis showed a significant difference of distance ($P < 0.001$) from dorsal axis between *afp4b-tb-miMO* ($22 \pm 6^\circ$) embryos and *afp4b-tb-MO* morphants ($68 \pm 9^\circ$) at 10 hpf (Fig. 8M), implicating that AFP4b might be related to convergent movement of lateral cells towards the dorsal side.

To measure the relationship between AFP4b and dorsal extension movement, a group of cells within the dorsal embryonic shield was marked at 6 hpf (Fig. 8G, J), and the movement of labeled cells was recorded at 8 hpf and 10 hpf. In both the *afp4b-tb-miMO* embryos and the *afp4b-tb-MO* morphants at 10 hpf, the marked cells were similarly distributed in the dorsal axial cells, and only a slight dorsal extension delay was observed in the *afp4b-tb-MO* morphants (Fig. 8G-L). A quantitative and statistical analysis also showed a slight reduction ($P < 0.05$) in the dorsal extension of the *afp4b-tb-MO* morphants ($634 \pm 36 \mu\text{m}$) relative to the *afp4b-tb-miMO* embryos ($735 \pm 46 \mu\text{m}$) (Fig. 8N). Together, these data indicate that AFP4b is primarily related to convergence movement.

Discussion

In this study, we have identified two head-to-tail tandem duplicated *afp4* genes (*afp4a* and *afp4b*) from gibel carp and zebrafish, and found that they possess similar genomic structures and protein sequences. Comparison of cDNA sequences between *afp4a* and *afp4b* shows high similarity in their ORF sequences, whereas significant differences exist in their UTR sequences and promoter sequences. RT-PCR analysis and WISH have revealed differential expression patterns and dynamic changes between *afp4a* and *afp4b* during embryogenesis, early larval development and adults. Thereby, we have found for the first time that both *afp4a* and *afp4b* are specifically expressed in YSL, but the later expressed *afp4b* exists only in embryogenesis, whereas *afp4a* expresses continuously in YSL and digestive system from early embryos to adults. Subsequently, we have studied the roles of AFP4a and AFP4b by using *afp4a*-specific and *afp4b*-specific morpholino knockdown approaches, and found that AFP4a and AFP4b contribute to early morphogenetic movements during zebrafish embryogenesis. Moreover, we have observed that the YCL microtubule cytoskeleton is disturbed in the *afp4a* morphants, while the actin cytoskeleton is not affected in the *afp4a* morphants, suggesting that AFP4a might participate in epiboly progression by stabilizing YCL microtubules. In addition, we have revealed that AFP4b is required for CE movement without affecting dorsoventral axis patterning, and demonstrated that AFP4b is primarily related to convergence movement. Therefore, this current study has confirmed that both

AFP4a and AFP4b are key regulators during zebrafish embryogenesis, and contribute to epiboly progression and convergence movement, respectively.

AFP4 was firstly isolated from the serum of longhorn sculpin in 1997 [23], and genomic structure of *afp4* had not been described until 2011 by Lee et al [25]. Previously, two *afp4* homologs have been reported from databases of three-spined stickleback (*Gasterosteus aculeatus*) and Atlantic salmon (*Salmo salar*) [25], but their distributions in the chromosomes have not been clarified. Here, for the first time, we have shown the genomic organization and the head-to-tail tandem distribution of the two duplicated *afp4s* in gibel carp and zebrafish. Gene duplication has been believed to be a major evolutionary driving force for organism complexity, and expression divergence has been proposed as the first step of functional divergence between duplicate genes [51]. The *afp4a* and *afp4b* are highly similar in their ORFs, but significant differences are found in their UTR sequences and promoter sequences, and differential expression patterns between *afp4a* and *afp4b* are also observed during their embryogenesis and early larval development. These differences should be consistent with their functional divergence. Previous studies have demonstrated that the *cis*-regulatory elements in the promoters can result in expression divergence [52] and the divergent sequences in 3' UTR also affect the expression pattern of duplicate genes [53, 54].

Along with AFP4s have been identified in temperate, subtropical and tropical fishes that have no need to prevent freezing [20, 24, 25], their biological roles have been speculated to bind to lipid or ligand other than ice because of the helix bundle structure similarity to certain apolipoproteins (Apos) [24, 26, 28], but the exact physiological functions have been unknown up to the present. Our current study has revealed the biological roles of AFP4a and AFP4b in embryonic development, and has confirmed that AFP4a and AFP4b contribute to epiboly progression and convergence movement during early zebrafish embryogenesis. Recently, some Apos, such as Apo-14 [55, 56], ApoA-II [57], ApoB [58], ApoC1 [45], have been also reported to participate in embryonic morphogenesis and organogenesis in gibel carp and zebrafish. Significantly, homological searches also show about 20% identities between AFP4s and some Apos that include mammalian ApoA-II and fish Apo-14, and the conserved amphipathic alpha-helices within AFP4s are also a common property in Apos. Therefore, we propose that *afp4s* might share a common ancestral gene with some *apos* genes, and still maintain the original function in temperate, subtropical and tropical fishes. In addition, *afp4a* and *afp4b* show similar expression patterns with Apo-14 [55]

and ApoC1 [45] during embryogenesis, and all of them are expressed in YSL. As it has been previously reported that some genes expressed in YSL function during early embryonic morphogenesis [45, 55, 57-60], AFP4a and AFP4b also play the related roles.

Another significant finding in this study is about the association between AFP4a and YCL microtubule cytoskeleton, because our results have revealed that the *afp4a*-MO morphants display an obvious defect in epiboly progression, and YCL microtubule arrays are less stable in *afp4a*-MO morphants. Previous studies have indicated that microtubule arrays in YCL are important drive of epiboly, and their homeostasis is crucial for normal epibolic movement [47, 48]. Two groups of related factors have been identified. The first group, which can stabilize YCL microtubules, includes Cyp11a1 [6] and calcium channel β 4 subunits (CACNB4) [60]. The second group, which are involved in microtubules organization, includes pou domain, class 5, transcription factor 1 (Pou5f1) [61] and eomesodermin A (Eomesa) [62]. Of these epiboly mutants and morphants, *afp4a*-MO morphants most closely resemble *cyp11a1*-MO morphants. Firstly, *afp4a* and *cyp11a1* have the common expression domain in YSL. Secondly, they both display serious epibolic defect and slight CE defect, but do not change germ layer patterning and involution. Thirdly, stability of YCL microtubules is lowered in both embryos. In addition, pregnenolone, the catalytic product of Cyp11a1, can partially rescue the epibolic defect of AFP4a-knockdown embryos. Our study indicates that AFP4a either directly or indirectly stabilizes the microtubules in YCL, which extends our knowledge of YCL microtubule regulation.

Supplementary Material

Figures S1 - S4, Tables S1 - S2.

<http://www.ijbs.com/v10p0715s1.pdf>

Abbreviations

AFP: Antifreeze protein; AFP4: type-IV antifreeze proteins; *afp4*: type-IV antifreeze protein gene; *Cag*: *Carassius auratus gibelio*; *Dr*: *Danio rerio*; *Cagafp4*: *afp4* in gibel carp; *Drafaf4s*: *afp4s* in zebrafish; YSL: yolk syncytial layer; YCL: yolk cytoplasmic layer; CE: convergence and extension; RACE: rapid amplification of cDNA ends; WT: wild type; qPCR: Real-time PCR; ML: maximum likelihood; WISH: whole-mount *in situ* hybridization; SD: standard deviation; ANOVA: analysis of variance; UTR: untranslated region; ORF: open reading frame; UV: ultraviolet; hpf: hours postfertilization; EVL: enveloping layer; Apo: apolipoprotein.

Acknowledgements

This work was funded by the National Key Basic Research Program of China (2010CB126301), the Strategic Priority Research Program of the Chinese Academy of Sciences (XDA08030201), the earmarked fund for Modern Agro-industry Technology Research System (NYCYTX-49), the Innovation Project of Chinese Academy of Sciences (KSCX3-EW-N-04), and the Autonomous Project of the State Key Laboratory of Freshwater Ecology and Biotechnology (2011FBZ17).

Competing Interests

The authors have declared that no competing interest exists.

References

- Keller R. Shaping the vertebrate body plan by polarized embryonic cell movements. *Science*. 2002; 298: 1950-4.
- Kimmel CB, Ballard WW, Kimmel SR, Ullmann B, Schilling TF. Stages of embryonic development of the zebrafish. *Dev Dyn*. 1995; 203: 253-310.
- Solnica-Krezel L, Sepich DS. Gastrulation: making and shaping germ layers. *Annu Rev Cell Dev Biol*. 2012; 28: 687-717.
- Solnica-Krezel L. Gastrulation in zebrafish – all just about adhesion? *Curr Opin Genet Dev*. 2006; 16: 433-41.
- Rohde LA, Heisenberg CP. Zebrafish gastrulation: cell movements, signals, and mechanisms. *Int Rev Cytol*. 2007; 261: 159-92.
- Hsu HJ, Liang MR, Chen CT, Chung BC. Pregnenolone stabilizes microtubules and promotes zebrafish embryonic cell movement. *Nature*. 2006; 439: 480-3.
- Schwend T, Loucks EJ, Snyder D, Ahlgren SC. Requirement of Npc1 and availability of cholesterol for early embryonic cell movements in zebrafish. *J Lipid Res*. 2011; 52: 1328-44.
- Yin C, Ciruna B, Solnica-Krezel L. Convergence and extension movements during vertebrate gastrulation. *Curr Top Dev Biol*. 2009; 89: 163-92.
- Dong CH, Yang ST, Yang ZA, Zhang L, Gui JF. A C-type lectin associated and translocated with cortical granules during oocyte maturation and egg fertilization in fish. *Dev Biol*. 2004; 265: 341-54.
- Peng JX, Xie JL, Zhou L, Hong YH, Gui JF. Evolutionary conservation of *Dazl* genomic organization and its continuous and dynamic distribution throughout germline development in gynogenetic gibel carp. *J Exp Zool Part B (Mol Dev Evol)*. 2009; 312B: 855-71.
- Wu N, Yue HM, Chen B, Gui JF. Histone H2A has a novel variant in fish oocytes. *Biol Reprod*. 2009; 81: 275-83.
- Yue HM, Li Z, Wu N, Liu Z, Wang Y, Gui JF. Oocyte-specific H2A variant H2af1o is required for cell synchrony before mid-blastula transition in early zebrafish embryos. *Biol Reprod*. 2013; 89: 82.
- Gui JF, Zhu ZY. Molecular basis and genetic improvement of economically important traits in aquaculture animals. *Chin Sci Bull*. 2012; 57: 1751-60.
- Zhou L, Wang Y, Gui JF. Genetic evidence for gynochoristic reproduction in gynogenetic silver crucian carp (*Carassius auratus gibelio* Bloch) as revealed by RAPD assays. *J Mol Evol*. 2000; 51: 498-506.
- Yang L, Gui JF. Positive selection on multiple antique allelic lineages of transferrin in the polyploid *Carassius auratus*. *Mol Biol Evol*. 2004; 21: 1264-77.
- Gui JF, Zhou L. Genetic basis and breeding application of clonal diversity and dual reproduction modes in polyploid *Carassius auratus gibelio*. *Sci China Life Sci*. 2010; 53: 409-15.
- Wang ZW, Zhu HP, Wang D, Jiang FF, Guo W, Zhou L, et al. A novel nucleo-cytoplasmic hybrid clone formed via androgenesis in polyploid gibel carp. *BMC Res Notes*. 2011; 4: 82.
- Jiang FF, Wang ZW, Zhou L, Jiang L, Zhang XJ, Apalikova OV, et al. High male incidence and evolutionary implications of triploid form in northeast Asia *Carassius auratus* complex. *Mol Phylogenet Evol*. 2013; 66: 350-9.
- Zhai YH, Zhou L, Wang Y, Wang ZW, Li Z, Zhang XJ, et al. Proliferation and resistance difference of a liver-parasitized myxosporean in two different gynogenetic clones of gibel carp. *Parasitol Res*. 2014; 113: 1331-41.
- Liu JX, Zhai YH, Gui JF. Molecular characterization and expression pattern of AFP4 during embryogenesis in gibel carp (*Carassius auratus gibelio*). *Mol Biol Rep*. 2009; 36: 2011-8.
- Doxey AC, Yaish MW, Griffith M, McConkey BJ. Ordered surface carbons distinguish antifreeze proteins and their ice-binding regions. *Nat Biotechnol*. 2006; 24: 852-5.
- Ewart K, Lin Q, Hew C. Structure, function and evolution of antifreeze proteins. *Cell Mol Life Sci*. 1999; 55: 271-83.
- Deng G, Andrews DW, Laursen RA. Amino acid sequence of a new type of antifreeze protein, from the longhorn sculpin *Myoxocephalus octodecemspinosis*. *FEBS Lett*. 1997; 402: 17-20.

24. Gauthier SY, Scotter AJ, Lin FH, Baardsnes J, Fletcher GL, Davies PL. A re-evaluation of the role of type IV antifreeze protein. *Cryobiology*. 2008; 57: 292-6.
25. Lee JK, Kim YJ, Park KS, Shin SC, Kim HJ, Song YH, et al. Molecular and comparative analyses of type IV antifreeze proteins (AFPIVs) from two Antarctic fishes, *Pleuragramma antarcticum* and *Notothenia coriiceps*. *Comp Biochem Physiol B Biochem Mol Biol*. 2011; 159: 197-205.
26. Deng G, Laursen RA. Isolation and characterization of an antifreeze protein from the longhorn sculpin, *Myoxocephalus octodecemspinosis*. *Biochim Biophys Acta*. 1998; 1388: 305-14.
27. Goetz FW, McCauley L, Goetz GW, Norberg B. Using global genome approaches to address problems in cod mariculture. *Ices J Mar Sci*. 2006; 63: 393-9.
28. Breton TS, Anderson JL, Goetz FW, Berlinsky DL. Identification of ovarian gene expression patterns during vitellogenesis in Atlantic cod (*Gadus morhua*). *Gen Comp Endocr*. 2012; 179: 296-304.
29. Celik Y, Drori R, Pertaya-Braun N, Altan A, Barton T, Bar-Dolev M, et al. Microfluidic experiments reveal that antifreeze proteins bound to ice crystals suffice to prevent their growth. *Proc Natl Acad Sci USA*. 2013; 110: 1309-14.
30. Fletcher GL, Hew CL, Davies PL. Antifreeze proteins of teleost fishes. *Annu Rev Physiol*. 2001; 63: 359-90.
31. Cheng C-HC, Detrich HW. Molecular ecophysiology of Antarctic notothenioid fishes. *Philos T Roy Soc B*. 2007; 362: 2215-32.
32. Geng FS, Zhou L, Gui JF. Construction and characterization of a BAC library for *Carassius auratus gibelio*, a gynogenetic polyploid fish. *Anim Genet*. 2005; 36: 535.
33. Xu H, Lim M, Dwarakanath M, Hong Y. Vasa identifies germ cells and critical stages of oogenesis in the Asian seabass. *Int J Biol Sci*. 2014; 10: 225-35.
34. Tamura K, Stecher G, Peterson D, Filipski A, Kumar S. MEGA6: molecular evolutionary genetics analysis version 6.0. *Mol Biol Evol*. 2013; 30: 2725-9.
35. Abascal F, Zardoya R, Posada D. ProtTest: selection of best-fit models of protein evolution. *Bioinformatics*. 2005; 21: 2104-5.
36. Westerfield M. The zebrafish book: a guide for the laboratory use of zebrafish (*Danio rerio*). Eugene: University of Oregon Press; 1995.
37. Huang W, Zhou L, Li Z, Gui JF. Expression pattern, cellular localization and promoter activity analysis of ovarian aromatase (Cyp19a1a) in protogynous hermaphrodite red-spotted grouper. *Mol Cell Endocrinol*. 2009; 307: 224-36.
38. Mei J, Zhang QY, Li Z, Lin S, Gui JF. *C1q-like* inhibits *p53*-mediated apoptosis and controls normal hematopoiesis during zebrafish embryogenesis. *Dev Biol*. 2008; 319: 273-84.
39. Mei J, Yue HM, Li Z, Chen B, Zhong JX, Dan C, et al. *C1q-like* factor, a target of miR-430, regulates primordial germ cell development in early embryos of *Carassius auratus*. *Int J Biol Sci*. 2014; 10: 15-24.
40. Li Z, Korzh V, Gong Z. Localized *rhp4* expression in the yolk syncytial layer plays a role in yolk cell extension and early liver development. *BMJ Dev Biol*. 2007; 7: 117.
41. Lou QY, He JY, Hu L, Yin Z. Role of *lhx2* in the noncanonical Wnt signaling pathway for convergence and extension movements and hypaxial myogenesis in zebrafish. *BBA-Mol Cell Res*. 2012; 1823: 1024-32.
42. Zhong JX, Zhou L, Li Z, Wang Y, Gui JF. Zebrafish Noxa promotes mitosis in early embryonic development and regulates apoptosis in subsequent embryogenesis. *Cell Death Differ*. 2014; 21: 1013-24.
43. Cheng JC, Miller AL, Webb SE. Organization and function of microfilaments during late epiboly in zebrafish embryos. *Dev Dyn*. 2004; 231: 313-23.
44. Köppen M, Fernandez BG, Carvalho L, Jacinto A, Heisenberg CP. Coordinated cell-shape changes control epithelial movement in zebrafish and *Drosophila*. *Development*. 2006; 133: 2671-81.
45. Wang Y, Zhou L, Li Z, Li WH, Gui JF. Apolipoprotein C1 regulates epiboly during gastrulation in zebrafish. *Sci China Life Sci*. 2013; 56: 975-84.
46. Carvalho L, Heisenberg CP. The yolk syncytial layer in early zebrafish development. *Trends Cell Biol*. 2010; 20: 586-92.
47. Strahle U, Jesuthasan S. Ultraviolet irradiation impairs epiboly in zebrafish embryos: evidence for a microtubule-dependent mechanism of epiboly. *Development*. 1993; 119: 909-19.
48. Solnica-Krezel L, Driever W. Microtubule arrays of the zebrafish yolk cell: organization and function during epiboly. *Development*. 1994; 120: 2443-55.
49. Bakkers J, Kramer C, Pothof J, Quaedvlieg NEM, Spaink HP, Hammerschmidt M. Has2 is required upstream of Rac1 to govern dorsal migration of lateral cells during zebrafish gastrulation. *Development*. 2004; 131: 525-37.
50. Zhu S, Liu L, Korzh V, Gong Z, Low BC. RhoA acts downstream of Wnt5 and Wnt11 to regulate convergence and extension movements by involving effectors Rho Kinase and Diaphanous: Use of zebrafish as an *in vivo* model for GTPase signaling. *Cell Signal*. 2006; 18: 359-72.
51. Ohno S. Evolution by gene duplication. New York: Springer-Verlag; 1970.
52. Li J, Yuan Z, Zhang Z. Revisiting the contribution of *cis*-elements to expression divergence between duplicated genes: the role of chromatin structure. *Mol Biol Evol*. 2010; 27: 1461-6.
53. Tong Y, Zheng K, Zhao SF, Xiao GX, Luo C. Sequence divergence in the 3'-untranslated region has an effect on the subfunctionalization of duplicate genes. *J Exp Zool Part B (Mol Dev Evol)*. 2012; 318B: 531-44.
54. Decembrini S, Andreazzoli M, Vignali R, Barsacchi G, Cremisi F. Timing the generation of distinct retinal cells by homeobox proteins. *PLoS Biol*. 2006; 4: e272.
55. Xia JH, Liu JX, Zhou L, Li Z, Gui JF. Apo-14 is required for digestive system organogenesis during fish embryogenesis and larval development. *Int J Dev Biol*. 2008; 52: 1089-98.
56. Choudhury M, Yamada S, Komatsu M, Kishimura H, Ando S. Homologue of mammalian apolipoprotein A-II in non-mammalian vertebrates. *Acta Bioch Bioph Sin*. 2009; 41: 370-8.
57. Zhang T, Yao S, Wang P, Yin C, Xiao C, Qian M, et al. Apoa-II directs morphogenetic movements of zebrafish embryo by preventing chromosome fusion during nuclear division in yolk syncytial layer. *J Biol Chem*. 2011; 286: 9514-25.
58. Seth A, Machingo QJ, Fritz A, Shur BD. Core fucosylation is required for midline patterning during zebrafish development. *Dev Dyn*. 2010; 239: 3380-90.
59. Chen SR, Kimelman D. The role of the yolk syncytial layer in germ layer patterning in zebrafish. *Development*. 2000; 127: 4681-9.
60. Ebert AM, McAnelly CA, Srinivasan A, Linker JL, Horne WA, Garrity DM. Ca²⁺ channel-independent requirement for MAGUK family CACNB4 genes in initiation of zebrafish epiboly. *Proc Natl Acad Sci USA*. 2008; 105: 198-203.
61. Lachnit M, Kur E, Driever W. Alterations of the cytoskeleton in all three embryonic lineages contribute to the epiboly defect of Pou5f1/Oct4 deficient *MZspg* zebrafish embryos. *Dev Biol*. 2008; 315: 1-17.
62. Du S, Draper BW, Mione M, Moens CB, Bruce A. Differential regulation of epiboly initiation and progression by zebrafish Eomesodermin A. *Dev Biol*. 2012; 362: 11-23.